

Contents lists available at [ScienceDirect](#)

Journal of Hydrology

journal homepage: www.elsevier.com/locate/jhydrol

Seasonal variation of high elevation groundwater recharge as indicator of climate response

Daniel C. Segal^{a,*}, Jean E. Moran^a, Ate Visser^b, Michael J. Singleton^b, Bradley K. Esser^b

^a California State University, East Bay, Hayward, CA, United States

^b Lawrence Livermore National Laboratory, Livermore, CA, United States

ARTICLE INFO

Article history:

Received 15 November 2013

Received in revised form 21 October 2014

Accepted 22 October 2014

Available online xxx

This manuscript was handled by Corrado Corradini, Editor-in-Chief, with the assistance of Xunhong Chen, Associate Editor

Keywords:

Climate impacts

Groundwater hydrology

Infiltration

Water supply

Isotopes

SUMMARY

High elevation groundwater basins in the western United States are facing changes in the amount and timing of snowmelt due to climate change. The objective of this study is to examine seasonal variability in a high elevation aquifer (Martis Valley Watershed near Truckee, CA) by analyzing (1) tritium and helium isotopes to determine groundwater sources and age, (2) dissolved noble gases to determine recharge temperatures and excess air concentrations. Recharge temperatures calculated at pressures corresponding to well head elevations are similar to mean annual air temperatures at lower elevations of the watershed, suggesting that most recharge is occurring at these elevations, after equilibrating in the vadose zone. The groundwater flow depth required to increase the water temperature from the recharge temperature to the discharge temperature was calculated for each well assuming a typical geothermal gradient. Groundwater samples contain large amounts of excess helium from terrigenous sources, including mantle helium and radiogenic helium. Terrigenous helium and tritium concentrations are used to determine the amount of mixing between the younger and older groundwater sources. Many of the wells sampled show a mix of groundwater ages ranging from >1000s of years old to groundwater with tritium concentrations that are in agreement with tritium in modern day precipitation. Higher seasonal variability found in wells with younger groundwater and shallower flow depths indicates that the recent recharge most vulnerable to climate impacts helps to supplement the older, less sustainable waters in the aquifer during periods of increased production.

© 2014 Elsevier B.V. All rights reserved.

1. Introduction

The western United States continues to rely heavily on groundwater to support population growth and agriculture making it critically important to understand how groundwater recharge will be impacted by predicted climate change (Green et al., 2011). Overall, regional groundwater recharge may increase or decrease as a result of higher predicted temperatures (Earman and Dettinger, 2007). However, groundwater recharge has been shown to be vulnerable to the effects of climate, especially in arid and semiarid regions (Aguilera and Murillo, 2009; Ajami et al., 2012; Barthel et al., 2009; Novicky et al., 2010). Alpine and subalpine groundwater basins in California may be particularly affected since they receive most of their groundwater recharge from seasonal snowpack melting. Even modest increases in temperature predicted by climate change have the potential to cause a greater proportion of precipitation in Califor-

nia to occur as rain, decrease the amount of snowpack in the Sierra Nevada, and shift the snowmelt hydrograph to an earlier and sharper peak (Earman and Dettinger, 2007). This will increase the likelihood of flooding events and likely cause a decrease in groundwater recharge of snowmelt, since there will be less total snowmelt and more snowmelt will leave the watershed as surface water. Climate change presents a challenge to managing the water supply, since it will have an effect on how much groundwater is recharging, where it is recharging, and by what mechanism recharge is occurring (Manning et al., 2012). One way of assessing the vulnerability of an aquifer system to relatively sudden shifts in recharge amount and location is to examine the degree of seasonal variability in the characteristics of the water mass produced at wells. Seasonal variability can include both natural and anthropogenic causes, such as variations in pumping rates and groundwater abstraction. By understanding current seasonal groundwater recharge conditions and residence times in high elevation basins where climate change is likely to affect precipitation and runoff, we can assess the vulnerability of mountain aquifers to climate change (Earman and Dettinger, 2007; Singleton and Moran, 2010).

* Corresponding author at: Chevron Energy Technology Company, San Ramon, CA, United States.

E-mail address: danielsegal@chevron.com (D.C. Segal).

Dissolved noble gases and isotope analysis have the potential to add new and unique information to aid in assessing groundwater vulnerability to climate change. Noble gas concentrations are used to examine recharge conditions, including recharge temperatures (Aeschbach-Hertig et al., 2000; Stute et al., 1995a) and excess air concentrations (Ingram et al., 2007; Wilson and McNeill, 1997). Tritium and helium isotope measurements can be used to evaluate the apparent age of a groundwater sample that is less than 50 years old, if circumstances allow for quantification of the various helium components (Poreda et al., 1988; Schlosser et al., 1988; Takaoka and Mizutani, 1987).

Previous studies have used noble gases and other environmental tracers to examine the vulnerability of mountain alluvial aquifers to climate change. Singleton and Moran (2010) identified zones of very young groundwater and pointed out their sensitivity to changing recharge conditions that might result from short-term climate variations. Manning et al. (2012) observed a general trend of increasing groundwater age over the past 13 years and attributed this to declining recharge rates due to recent warming and declining snowpack. This study utilizes the novel approach of examining seasonal variations in groundwater age and recharge temperature to identify the most seasonally dynamic parts of an aquifer, which would presumably be the most susceptible to short-term climate variations. Specifically, we use tritium and helium isotopes and dissolved noble gases to examine seasonal variability in groundwater age and recharge source for samples collected from wells in the Martis Valley near Truckee, CA in the Sierra Nevada Mountains. We then use this information to address two key questions important for effective management of this and other mountain alluvial aquifers under changing climate conditions: (1) Will mountain aquifers with large storage capacity, like the Martis Valley, be well-buffered against short-term fluctuations in the availability of recharge? (2) What portion of recharge occurs through exposed fractured bedrock at the highest-elevations in the watershed where most of the snowpack resides, the recharge component most directly impacted by warming and declining snow amounts?

2. Methods

2.1. Study site

Martis Valley, in the Sierra Nevada, has been identified as a region likely to face water shortages in the future (Coats, 2010) and was selected to study how climate change is impacting groundwater supply. Martis Valley, at over 1800 m above sea level, is unique for a high elevation basin, since there are 14 production wells producing large volumes (1.15×10^7 m³/year) of groundwater from various locations and depths in the aquifer (Fig. 1). Martis Valley's economy is largely sustained by tourism (Dean Ruyan Associates, 2013) and groundwater is the exclusive source for providing drinking water to the town of Truckee and the surrounding region, irrigation for golf courses in summer and for creating artificial snow at ski resorts in winter. Despite heavy reliance upon and development of groundwater resources, relatively little is known about the groundwater system.

Martis Valley is a structural basin north of Lake Tahoe in the Walker Lane Belt shear zone, a transitional zone between the Sierra Nevada Mountains and the Basin and Range Geomorphic Provinces (Brown and Caldwell, 2013). The lowest terrace in the valley floor is at 1737 m elevation. Mountains rise dramatically to the south including the 2665 m elevation Martis Peak. The Martis Valley groundwater basin lies between the Sierra Nevada crest in the west and the Carson Range to the east. Extensional Basin and Range-style normal faulting, as well as Walker Lane Belt associated strike-slip

faulting formed this structural valley during the Pliocene and early Pleistocene as the Sierra Nevada uplifted about 1524 m relative to the graben. Most structural development has occurred during the last five million years and active faulting continues to this day. Four major glacial events shaped the topography of Martis Valley during the Pleistocene. Glacial moraines and outwash plain sediments from the Tahoe and Tioga glaciations fill much of the Martis Valley basin (Fram et al., 2009).

The Martis Valley watershed occupies an area of 147.6 km² in Nevada and Placer counties. The Truckee River flows SW to NE across Martis Valley and is controlled upstream by a dam at the edge of Lake Tahoe. Flows in the Truckee River are managed by the Truckee River Operating agreement (Coulter et al., 2009). The groundwater bearing units in Martis Valley are up to 300 m thick and are comprised of interlayered Miocene to late Pleistocene volcanic and sedimentary deposits. Low-permeability Miocene volcanic rocks form the base of the water bearing units. Basin-fill volcanic units include andesite lava, tuff, and breccia. Sediments originating from the volcanic and volcanoclastic units surrounding Martis Valley comprise the glacial, lacustrine, and fluvial sedimentary deposits. These sedimentary deposits provide the most groundwater storage and best opportunity for extraction. These units also include relatively impermeable laterally extensive clay and silt layers (California Department of Water Resources, 2006). Roughly half of the surface of Martis Valley is covered in glacial outwash sediments that are up to 46 m thick. The basin depocenter, where sediments are up to 300 m thick, is located to the south of the Truckee River near the middle of the watershed area. The basin's stratigraphy is divided into lower and upper aquifer systems. The lower aquifer system is found in the Truckee formation while the upper aquifer system consists of the shallower glacial and alluvium deposits. These units are thought to have limited interconnectivity, with the Lousestown volcanic units acting as a barrier to flow. Some wells were historically artesian in southern Martis Valley, indicating confined conditions over some portion of the aquifer system. These wells are also situated near faults, which are interpreted as barriers to groundwater flow (Brown and Caldwell, 2013). Thermal springs are found in this region, adjacent to the recently-mapped Polaris Fault (Hunter et al., 2011).

Annual groundwater levels have remained relatively constant from 1990 through 2000 with seasonal water level variations often exceeding 3 m. The water level elevation is controlled by the hydrogeologic units' complex stratigraphy, topography, and groundwater flow barriers. In general, hydraulic gradients determined from groundwater elevations indicate that groundwater flow in the basin is toward the Truckee River (California Department of Water Resources, 2006; Hydro-Search, 1995). Groundwater storage for Martis Valley Basin has been estimated at 5.97×10^8 m³ with an average specific yield of 0.05. Annual groundwater recharge is estimated at 2.9×10^7 m³ (0.20 m) from precipitation, including snowmelt, and 2.9×10^6 m³ (0.02 m) from artificial recharge at a wastewater treatment facility east of Truckee. Urban extraction of groundwater is estimated at 8.71×10^6 m³ (0.06 m) per year, with an additional 1.57×10^6 m³ (0.01 m) extracted to irrigate golf courses. Mountain-block recharge and subsurface outflow are estimated at 6.6×10^6 m³ (0.04 m) and 2.2×10^7 m³ (0.15 m) per year, respectively (Nimbus Engineers, 2001). Desert Research Institute's Martis Valley integrated groundwater, surface water, and climate change model (Huntington et al., 2013) provides a more recent groundwater recharge estimate of 4.0×10^7 – 4.3×10^7 m³/year (0.27–0.30 m/year), consisting of the sum of shallow infiltrated water that discharges to the Truckee River and its tributaries plus deep percolation to aquifers tapped by water supply wells. While current annual groundwater extraction is only about 30% of groundwater recharge, future scenarios predict higher demand and potentially lower recharge.

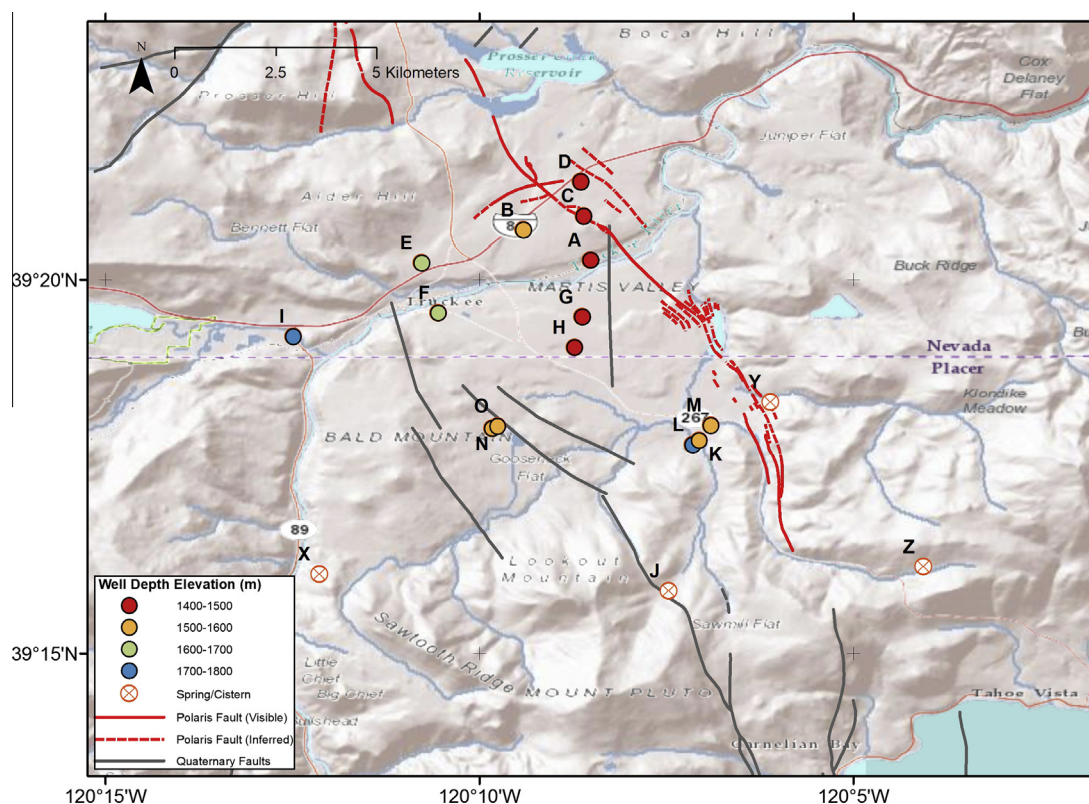


Fig. 1. Martis Valley Shaded Relief Map. Letter labels display the locations of the sampled production wells, springs, and cistern. Locations are labeled A–O and wells are color coded according to the elevation of the lowest depth of the well. The locations of the active Polaris Fault and local quaternary faults are also shown. (For interpretation of the references to color in this figure legend, the reader is referred to the web version of this article.)

Snow, rain, and temperature are measured at the USFS Truckee Ranger Station and at SNOTEL Station Truckee #2 where the mean annual air temperature is 7 °C. Temperature ranges from average lows of –9 °C in December to average highs of 28 °C in July. Mean annual precipitation varies from 1778 mm in the western portion of the basin to 582 mm in the northeastern portion of the basin. Martis Valley, being at lower elevation and situated in the eastern portion of the basin, receives precipitation on the low end of the stated range (<760 mm/year). Snow accounts for approximately 77% of the precipitation in the Truckee region (Stone and Lopez, 2009) with the balance supplied by summer thunderstorms and other rain events. A one hundred and ten year precipitation record indicates that dry periods (e.g., 1971–1978, 1987–1994), with precipitation up to 50% below the annual average, are of longer duration than wet periods (e.g., 1962–1965, 1982–1983), which are more extreme at up to 75% above the annual average (Brown and Caldwell, 2013). Tree ring and lake level studies show evidence of decades-long drought periods over the past 10,000 years (Kleppe et al., 2011). Climate change projections predict a shift from snowfall to rain at the valley floor elevation due to increasing global temperatures (Coats, 2010).

2.2. Sample collection and analytical methods

Tritium and dissolved noble gas samples were collected from 12 production wells (labeled A–O in Fig. 2) operated by Truckee–Donner Public Utility District, Northstar Community Services District, and the Placer County Water Agency. Many of these production wells have long well screens and/or multiple open intervals as shown in Fig. 5. Long, alternating perforated intervals allow high production rates in Martis Valley’s complex hydrogeological setting with variable layering of permeable and semi-permeable volcanic,

glacial, and alluvial deposits (Fram et al., 2009). Hydrostratigraphic units tapped by different well screen intervals have variable transmissivity, and further mixing in the wellbore results in a complex mixture of waters with variable geochemical signatures. Samples were also collected from three springs (the headwaters of Middle Martis Creek (Z), a spring draining eastward into the Truckee River upstream of Martis Valley (X), and a spring flowing near the Polaris Fault (Y).

Tritium samples were collected in 1 L glass bottles without filtration or preservatives. Tritium concentrations were determined on 500 g sub-samples by the ^3He in-growth method (approximately 25 day accumulation time) at Lawrence Livermore National Laboratory (Clarke et al., 1976; Surano et al., 1992).

Dissolved noble gas samples ($^3\text{He}/^4\text{He}$, He, Ne, Ar, Kr, Xe) were collected using clear Tygon tubing to connect the sample vessel (8 mm inner diameter copper tubing, 250 mm long) to the well-head of operating production wells. Water flowed for several minutes to purge air from the sample tube. The copper tubing was tapped lightly to dislodge bubbles and a visual inspection for bubbles was made. Close attention was paid to maintaining sufficient pressure in the sampling apparatus, and backpressure was applied when necessary to prevent escape of dissolved gas. The copper tube is pinched closed using steel clamps on either end to protect the sample from atmospheric contamination.

Copper tube samples for noble gas analysis were mounted on a multi-port gas handling manifold under vacuum at Lawrence Livermore National Laboratory. Reactive gases were removed with multiple reactive metal getters. Known quantities of isotopically enriched ^{22}Ne , ^{86}Kr and ^{136}Xe were added to provide internal standards. Noble gases were separated from one another using cryogenic adsorption. Helium isotopes were analyzed using a VG-5400 noble gas mass spectrometer. Neon, krypton and xenon

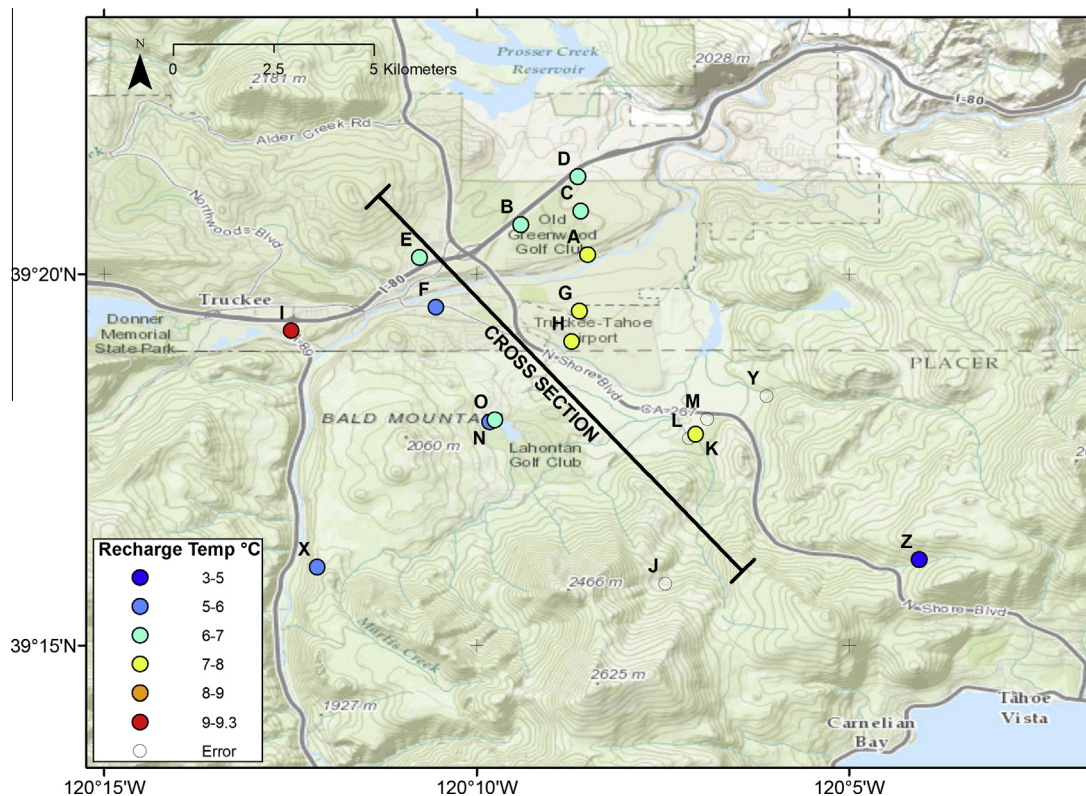


Fig. 2. Map of Martis Valley showing sample locations and recharge temperatures. Letter labels show the locations of the sampling sites. Sample locations are shown with calculated noble gas recharge temperatures, averaged from each sampling event. Also shown is the location of the cross section shown in Fig. 5. (Results of dissolved noble gas sampling from locations L, M, J, and spring Y are not valid due to poor sampling conditions.)

abundances were measured using a quadrupole mass spectrometer. The Ar abundance was determined by pressure measurement using a high-sensitivity capacitance manometer. The procedure was calibrated using water samples equilibrated with the atmosphere at a known temperature and air standards spiked with known quantities of the noble gases. Analytical uncertainties are approximately 1% for $^3\text{He}/^4\text{He}$, 2% for He, Ne, and Ar, and 3% for Kr and Xe. Errors for derived parameters such as groundwater age and recharge temperature are propagated using analytical errors for the individual measured quantities. A detailed description of the procedure is reported in Ekwurzel (2004) and Visser et al. (2013b).

Noble gas concentrations are used to calculate groundwater recharge temperatures and excess air concentrations, and groundwater ages are calculated using the tritium–helium method. Recharge temperature and excess air were calculated by fitting noble gas concentrations to partial re-equilibration (Stute et al., 1995b), closed equilibrium (Aeschbach-Hertig et al., 2008), and unfractionated (Heaton and Vogel, 1981) excess air models. The model that received the highest χ^2 probability for each sample was used to calculate the recharge temperature, excess air concentration, and other derived parameters.

3. Results and discussion

3.1. Tritium and dissolved noble gas data

Dissolved noble gas and tritium concentrations for Martis Valley groundwater samples are presented in Table 1. The derived parameters are shown in Table 2. Differing results from the same wells during winter (December 2011–January 2012), summer (June 2012), and fall (September 2012) sampling events reflect

the extent of seasonal variation in the sources of groundwater produced in the Martis Valley basin.

All well samples fit at least one of the excess air models with a probability of more than 18%. Excluding the spring samples, the cistern and open test hole samples, the three excess air models were evaluated by summing the chi-squared deviations and calculating the probability given the total number of degrees of freedom. The probability of the UA model is highest (99.9%) due to the lower number of free parameters. Both the CE and PR model perform well (70% and 78%). The high probability for the UA model indicates that the actual measurement accuracy is better than then estimated uncertainty. The derived parameters for each sample were calculated using the best fitting model (UA model, CE model or PR model).

3.2. Noble gas recharge temperatures and recharge area

Fig. 2 shows the calculated noble gas recharge temperatures in Martis Valley wells and springs. Recharge temperatures calculated here assume an atmospheric pressure that corresponds to the elevation at the well head. The effect of assuming higher recharge elevations is illustrated in Fig. 3.

There is a general pattern of lower recharge temperatures with increasing altitude in the mountains and foothills surrounding Martis Valley, and recharge temperatures are highest for wells on the valley floor. An anomalously high recharge temperature was found in the sample from Well I collected in September. This high recharge temperature is likely the result of mixing between local groundwater and a component of water from nearby Donner Creek or the quarries to the west.

Historical air temperature data from Martis Valley's two weather stations reveal a unique microclimate with each station

Table 1
Measured concentrations of tritium and dissolved noble gases.

Well ID	Well Type	Elevation (m asl)	Top (m bgs)	Bottom (m bgs)	Collection Date
A	Production	1753	82	274	6/19/2012
A	Production	1753	82	274	9/5/2012
B	Irrigation	1796	76	274	6/19/2012
B	Irrigation	1796	76	274	9/5/2012
C	Production	1820	140	415	1/19/2012
C	Production	1820	140	415	6/19/2012
C	Production	1820	140	415	9/5/2012
D	Production	1783	85	338	1/19/2012
D	Production	1783	85	338	6/19/2012
D	Production	1783	85	338	9/5/2012
E	Production	1823	38	183	1/19/2012
E	Production	1823	38	183	6/19/2012
E	Production	1823	38	183	9/5/2012
F	Production	1791	27	122	6/19/2012
F	Production	1791	27	122	9/5/2012
G	Production	1770	87	283	1/19/2012
G	Production	1770	87	283	6/19/2012
G	Production	1770	87	283	9/5/2012
H	Production	1796	30	313	1/19/2012
H	Production	1796	30	313	6/19/2012
H	Production	1796	30	313	9/5/2012
I	Irrigation	1797	15	61	6/20/2012
I	Irrigation	1797	15	61	9/5/2012
J	Cistern	2073	–	–	6/20/2012
K	Production	1783	66	244	12/19/2011
K	Production	1783	66	244	6/20/2012
K	Production	1783	66	244	9/6/2012
L	Test Well	1783	20	81	12/20/2011
L	Test Well	1783	20	81	6/20/2012
M	Test Well	1786	70	239	12/20/2011
M	Test Well	1786	70	239	6/20/2012
N	Production	1832	46	274	12/19/2011
N	Production	1832	46	274	6/20/2012
N	Production	1832	46	274	9/6/2012
O	Production	1830	43	274	12/19/2011
O	Production	1830	43	274	6/20/2012
O	Production	1830	43	274	9/6/2012
X	Spring	1939	–	–	10/29/2012
Y	Spring	1819	–	–	10/29/2012
Z	Spring	2221	–	–	10/29/2012

Well ID	Collection Date	^3H (pCi/L)	±	$^3\text{He}/^4\text{He}$ (10–6)	±	He (10–8 cm3STP/g)	±	Ne (10–7 cm3STP/g)	±	Ar (10–4 cm3STP/g)	±	Kr (10–8 cm3STP/g)	±	Xe (10–8 cm3STP/g)	±
A	6/19/2012	2.51	0.5	3.33	0.04	47.55	0.95	1.97	0.04	3.48	0.07	7.99	0.24	1.21	0.04
A	9/5/2012	1.77	0.75	3.33	0.05	44.45	0.89	2.03	0.04	3.49	0.07	8.05	0.24	1.21	0.04
B	6/19/2012	3.69	0.58	3.5	0.05	498	9.96	4.31	0.09	4.87	0.1	9.86	0.3	1.35	0.04
B	9/5/2012	–0.5	0.85	3.48	0.05	427.35	8.55	3.02	0.06	4.1	0.08	9.01	0.27	1.28	0.04
C	1/19/2012	2.15	0.52	2	0.03	7.72	0.15	2.42	0.06	3.74	0.07	8.6	0.26	1.37	0.04
C	6/19/2012	2.05	0.34	2.39	0.02	11.45	0.23	2.35	0.05	3.72	0.07	8.4	0.25	1.21	0.04
C	9/5/2012	1.42	0.43	2.79	0.04	15.87	0.32	2.31	0.05	3.69	0.07	8.47	0.25	1.18	0.04
D	1/19/2012	2.74	1	2.08	0.02	5.75	0.12	2.17	0.04	3.58	0.07	8.38	0.25	1.22	0.04
D	6/19/2012	3.28	0.96	3.15	0.02	77.2	1.54	3.49	0.07	4.33	0.09	9.4	0.28	1.28	0.04
D	9/5/2012	3.66	0.25	3.19	0.04	55.68	1.11	2.02	0.04	3.52	0.07	8.35	0.25	1.28	0.04
E	1/19/2012	3.14	0.56	2.63	0.02	258.41	5.17	1.87	0.06	3.41	0.07	8.18	0.25	1.19	0.04
E	6/19/2012	2.5	0.5	2.75	0.02	346	6.92	2.08	0.04	3.53	0.07	8.05	0.24	1.17	0.03
E	9/5/2012	2.36	0.4	2.61	0.06	227.08	4.54	1.98	0.04	3.5	0.07	8.34	0.25	1.24	0.04
F	6/19/2012	7.08	1.69	2.01	0.02	6.24	0.12	1.92	0.04	3.47	0.07	8.42	0.25	1.15	0.03
F	9/5/2012	8.93	0.52	1.77	0.02	5.48	0.11	1.98	0.04	3.52	0.07	8.5	0.25	1.27	0.04
G	1/19/2012	5.7	0.64	3.1	0.03	40.67	0.81	1.97	0.06	3.45	0.07	7.98	0.24	1.16	0.03
G	6/19/2012	4.2	0.52	3.22	0.03	43.98	0.88	1.98	0.04	3.52	0.07	8.28	0.25	1.15	0.03
G	9/5/2012	4.48	0.4	3.05	0.04	26.92	0.54	2.1	0.04	3.6	0.07	8.55	0.26	1.27	0.04
H	1/19/2012	4.26	0.57	2.73	0.05	16.76	0.34	2.85	0.09	3.95	0.08	8.51	0.26	1.2	0.04
H	6/19/2012	2.87	0.49	2.56	0.04	28.27	0.57	5.14	0.1	5.5	0.11	11.01	0.33	1.36	0.04
H	9/5/2012	2.14	0.79	2.27	0.04	24.58	0.49	6.62	0.13	7.48	0.15	13.32	0.4	1.72	0.05
I	6/20/2012	11.69	0.77	1.73	0.04	5.69	0.11	2.04	0.04	3.45	0.07	7.85	0.24	1.23	0.04
I	9/5/2012	10.44	0.54	1.65	0.02	5.64	0.11	1.99	0.04	3.18	0.06	7.4	0.22	1.04	0.03
J	6/20/2012	11.92	0.51	1.36	0.03	3.62	0.07	1.64	0.03	3.31	0.07	7.95	0.24	1.23	0.04
K	12/19/2011	0.14	0.34	3	0.05	23.2	0.46	3.45	0.07	4.25	0.08	8.85	0.27	1.24	0.04
K	6/20/2012	–0.37	0.44	3.12	0.05	23.3	0.47	3.24	0.06	4.13	0.08	8.67	0.26	1.23	0.04
K	9/6/2012	0.31	0.76	3.1	0.04	21.44	0.43	3.3	0.07	4.13	0.08	8.74	0.26	1.22	0.04
L	12/20/2011	0.55	0.52	1.38	0.01	6.07	0.12	2.11	0.05	3.64	0.07	8.39	0.25	1.27	0.04
L	6/20/2012	0.16	0.27	1.34	0.03	4.63	0.09	2	0.04	3.52	0.07	8.08	0.24	1.21	0.04

(continued on next page)

Table 1 (continued)

Well ID	Collection Date	^3H (pCi/L)	±	$^3\text{He}/^4\text{He}$ (10 ⁻⁶)	±	He (10–8 cm ³ STP/g)	±	Ne (10–7 cm ³ STP/g)	±	Ar (10–4 cm ³ STP/g)	±	Kr (10–8 cm ³ STP/g)	±	Xe (10–8 cm ³ STP/g)	±
M	12/20/2011	0.31	0.39	4.01	0.07	28.16	0.56	1.94	0.04	3.29	0.07	7.8	0.23	1.18	0.04
M	6/20/2012	-0.32	0.55	4.02	0.04	32.56	0.65	1.89	0.04	3.4	0.07	7.75	0.23	1.11	0.03
N	12/19/2011	5.22	0.51	1.34	0.01	5.13	0.1	2.38	0.05	3.69	0.07	8.67	0.26	1.28	0.04
N	6/20/2012	4.06	0.25	2.95	0.02	12.61	0.25	2.22	0.04	3.66	0.07	8.28	0.25	1.29	0.04
N	9/6/2012	4.73	2.31	2.87	0.04	11.9	0.24	2.21	0.04	3.68	0.07	8.61	0.26	1.3	0.04
O	12/19/2011	5.99	0.48	2.12	0.02	6.59	0.13	2.02	0.04	3.52	0.07	8.19	0.25	1.23	0.04
O	6/20/2012	5.23	0.42	2.07	0.02	6.63	0.13	2.14	0.04	3.62	0.07	8.21	0.25	1.29	0.04
O	9/6/2012	2.39	2.25	2.93	0.04	11.88	0.24	2.12	0.04	3.6	0.07	8.42	0.25	1.18	0.04
X	10/29/2012	9.72	0.57	1.45	0.03	3.88	0.08	1.79	0.04	3.41	0.07	8.3	0.25	1.22	0.04
Y	10/29/2012	-0.28	0.85	3.7	0.07	17.07	0.34	1.81	0.04	3.29	0.07	7.56	0.23	1.15	0.03
Z	10/29/2012	7.89	0.39	1.56	0.03	3.74	0.07	1.74	0.03	3.45	0.07	8.55	0.26	1.37	0.04

recording a similar mean annual air temperature (MAAT) despite a 159 m difference in elevation. Cold air flows down the slopes and into the valley causing somewhat anomalously low MAATs as these cool air masses pool on the valley floor. The Truckee Ranger Station at 1775 m elevation had a MAAT of 6.9 °C between 1993 and 2008 (National Climatic Data Center, 2011) while the Truckee #2 Snotel station at 1934 m elevation had a slightly higher MAAT of 7.2 °C between 1993 and 2008 (National Resources Conservation Service, 2013). The adiabatic lapse rate would predict the Snotel site to be 1 °C colder. The MAAT is representative of the temperature of the vadose zone below 2–3 m depth, which is nearly constant throughout the year (Flint et al., 2008). The typical thickness of the vadose zone for each well sampled was greater than 20 m, with the exception of Well I, having a 4 m vadose zone. Travel times through the vadose zone are likely long enough to allow infiltrating snowmelt to equilibrate at the MAAT. Assuming a recharge elevation of 1800 m, the median estimated recharge temperature of Martis Valley wells (7.1 °C) was close to the MAAT (6.9 °C) at the valley floor (Fig. 3). These recharge temperatures are higher than the temperature of snowmelt water, which would be close to 0 °C.

Assuming higher recharge elevations results in lower estimated recharge temperatures, on average by 3.2 °C per 1000 m for the unfractionated excess air model. Median recharge temperatures at assumed recharge elevations of 1900 and 2000 m are below the adiabatic lapse rate, and median recharge temperatures above 2200 m are above the adiabatic lapse rate. While recharge at higher elevations cannot be excluded for individual wells, this suggests that most groundwater sampled in this study recharged at the valley floor in thermal equilibrium with the vadose zone (Fig. 3). The relatively small range in calculated recharge temperatures for these wells suggests a common recharge elevation for most of the groundwater. The surface area at elevations above 1950 m is also quite small, making significant recharge from there unlikely. In practice, the range of possible recharge temperatures and the location of recharge are constrained by the local geography. However, lower recharge temperatures that would be calculated using elevations at the top of the watershed cannot be ruled out.

3.3. Groundwater flow path depths derived using geothermal heating

With the vast majority of precipitation falling as snow, the likely source for most groundwater recharge in Martis Valley is snowmelt, which is released from the snowpack in spring. Calculated noble gas recharge temperatures range between 5 and 11 °C, and are higher than would be expected for direct infiltration of snowmelt. Groundwater discharge temperatures are significantly higher than noble gas recharge temperatures. These differences reflect both surface and soil processes and deeper subsurface processes. In the near-subsurface, water temperature increases as snowmelt equilibrates to temperatures in the vadose zone (at a temperature close to mean

annual air temperature for that elevation) and eventually reaches the water table – these processes are reflected in the difference between the snow melting point and noble gas recharge temperature (the blue bar in Fig. 3). During subsurface transport, groundwater temperature increases due to geothermal heating, with the magnitude of heating potentially related to the depth of the flow path – this process is reflected in the difference between noble gas recharge temperature and well discharge temperature (the red¹ bar in Fig. 4).

Water moving through the subsurface transports heat and changes the subsurface temperature distribution. The rate of change of thermal energy in a parcel of groundwater is the sum of gravitational potential energy dissipation, heat transfer to/from the surface, and geothermal heating (Manga and Kirchner, 2004). In the case of Martis Valley sediments, conductive heat transport to/from the surface can be ignored because the advective rate of heat transport due to groundwater flow is likely much higher in the permeable aquifer materials. Also, the elevation difference between recharge and discharge, as indicated by noble gas recharge temperature analysis, is not large enough for the potential energy dissipation term to be significant. Heating of groundwater is therefore likely dominated by the geothermal heating component.

The thickness of groundwater bearing deposits in Martis Valley are estimated at up to 366 m (Fram et al., 2009). Assuming a geothermal gradient of 25 °C/km, groundwater flowing through the base of the water bearing deposits and warming to the ambient temperature is predicted to be 9 °C warmer than groundwater near the surface. In the samples analyzed for this study, groundwater discharge temperatures are greater than calculated noble gas recharge temperatures, by as much as 10 °C, an observation consistent with deep flow paths and warming during subsurface transport. If we assume that all warming occurred in the sedimentary basin, an estimated average flow depth for each well can be calculated by comparing the measured well discharge temperature to the calculated noble gas recharge temperature, and then determining the depth within the basin required to increase its recharge temperature to its discharge temperature, assuming a constant geothermal gradient of 25 °C/km, homogeneous thermal conductivity and a constant flow velocity. This would be a minimum flow depth if the heat added by geothermal warming is significantly diluted by advection of large volumes of water. Martis Valley is located between the Sierra Nevada, which has a low geothermal gradient, and the higher heat flow Basin and Range region. The geothermal gradient for Martis Valley was estimated to be similar to the continental geothermal gradient of 25 °C/km by comparing geothermal maps compiled by Southern Methodist University's Geothermal Lab (<http://www.google.org/egs/>, accessed March 2013).

¹ For interpretation of color in Fig. 4, the reader is referred to the web version of this article.

Table 2
Parameters derived from noble gas and tritium concentrations.

Well ID	Collection Date	Excess air Model [†]	Recharge Temp (°C)	± (°C)	ΔNe (%)	Excess air (10 ⁻³ cm ³ STP/g)	F (CE) or R (PR) –	Pχ ² (%)	³ H– ³ He Age (year)	±	⁴ He _{ter} (10 ⁻⁸ cm ³ STP/g)	±	R _{na} ^{**} (Ra)	R _{ter,min} ^{***} (Ra)	Flow depth (m)
A	6/19/2012	UA	7.2	0.6	17	1.6	–	67	Mantle He	–	42.9	1	2.56	2.49	206
A	9/5/2012	UA	7.3	0.6	21	2	–	69	Mantle He	–	39.6	0.9	2.58	2.53	233
B	6/19/2012	CE	6.6	0.7	157	18	0.08	73	Mantle He	–	486.9	10	2.56	2.55	311
B	9/5/2012	UA	6.1	0.6	79	7.4	–	98	>50	–	419.7	8.5	2.54	2.54	386
C	1/19/2012	PR	10.5	0.7	42	12.9	1.26	33	Mantle He	–	23.7	0.6	1.02	0.91	262
C	6/19/2012	CE	7.2	0.6	42	7	0.32	88	Mantle He	–	5.8	0.3	2.44	2.03	206
C	9/5/2012	PR	8.1	0.6	40	8	0.79	70	Mantle He	–	11.2	0.3	2.47	2.32	179
D	1/19/2012	UA	6.8	0.6	29	2.7	–	92	48	7	0.6	0.2	6.33	0.54	142
D	6/19/2012	UA	6.4	0.6	107	10	–	83	Mantle He	–	68.2	1.6	2.45	2.39	208
D	9/5/2012	UA	6	0.6	19	1.8	–	35	Mantle He	–	51	1.1	2.43	2.34	243
E	1/19/2012	UA	6.9	0.6	12	1.1	–	92	Mantle He	–	254	5.2	1.92	1.9	332
E	6/19/2012	UA	7.5	0.6	25	2.3	–	86	Mantle He	–	341	6.9	2	1.99	304
E	9/5/2012	UA	6.3	0.6	18	1.6	–	75	Mantle He	–	222.5	4.5	1.9	1.89	382
F	6/19/2012	PR	10	0.6	18	22.6	2.65	27	Mantle He	–	2.4	0.2	2.2	0.01	182
F	9/5/2012	UA	5.9	0.6	17	1.6	–	57	9	13	0.8	0.2	2.9	0.01	99
G	1/19/2012	UA	7.8	0.6	19	1.7	–	98	Mantle He	–	36	0.8	2.4	2.21	153
G	6/19/2012	PR	9.2	0.6	21	12.4	1.89	62	Mantle He	–	40	0.9	2.46	2.34	64
G	9/5/2012	UA	5.9	0.6	24	2.2	–	71	Mantle He	–	21.9	0.6	2.48	2.24	217
H	1/19/2012	CE	8.4	0.7	73	10.5	0.21	80	Mantle He	–	9.7	0.4	2.68	2.17	69
H	6/19/2012	PR	8.8	0.8	214	37.6	0.67	61	Mantle He	–	19	0.6	2.32	2.14	43
H	9/5/2012	CE	4.8	0.9	287	58.7	0.14	21	Mantle He	–	8.2	0.6	2.93	2.62	283
I	6/20/2012	UA	7.5	0.6	23	2	–	18	5	13	0.9	0.2	2.74	0.01	127
I	9/5/2012	UA	11.2	0.6	24	2.1	–	80	0	21	0.8	0.2	2.41	0.01	103
J	6/20/2012	UA	5.6	0.6	0	0	–	66	0	2	0	0.1	–	–	–
K	12/19/2011	UA	7.7	0.7	108	9.9	–	80	>50	–	14.2	0.5	2.91	2.91	419
K	6/20/2012	UA	7.7	0.6	95	8.7	–	75	>50	–	15	0.5	2.96	2.96	379
K	9/6/2012	UA	8	0.7	99	9.1	–	94	>50	–	12.9	0.5	3.06	3.06	411
L	12/20/2011	UA	5.9	0.6	25	2.3	–	77	>50	–	1.1	0.2	1.04	1.04	–
L	6/20/2012	UA	7	0.6	20	1.8	–	80	>50	–	0	0.2	–	–	–
M	12/20/2011	UA	8.4	0.6	18	1.6	–	21	>50	–	23.6	0.6	3.27	3.27	–
M	6/20/2012	CE	9.6	0.6	16	22.2	0.8	84	>50	–	28.2	0.7	3.21	3.21	–
N	12/19/2011	UA	6	0.6	42	3.8	–	52	0	3	0	0.2	–	–	59
N	6/20/2012	UA	5.9	0.6	32	2.9	–	28	Mantle He	–	7.3	0.3	2.96	2.31	99
N	9/6/2012	UA	5.4	0.6	31	2.8	–	61	Mantle He	–	6.6	0.3	2.95	2.03	137
O	12/19/2011	UA	6.6	0.6	21	1.9	–	82	23	15	1.8	0.2	2.98	0.01	67
O	6/20/2012	UA	6	0.6	27	2.5	–	23	27	12	1.5	0.2	3.21	0.01	90
O	9/6/2012	UA	6.7	0.6	27	2.5	–	68	Mantle He	–	6.8	0.3	2.96	2.12	93
X	10/29/2012	UA	5.8	0.6	7	0.7	–	89	7	2	0	0.1	–	–	–
Y	10/29/2012	UA	8.5	0.6	10	0.9	–	59	>50	–	12.8	0.4	3.22	3.22	–

[†] Excess air models include UA-unfractionated air, PR-partial re-equilibration, and CE-closed equilibrium.

^{**} R_{na}: isotope ratio of non-atmospheric (tritogenic plus terrigenic) helium.

^{***} R_{ter,min}: minimum isotope ratio of terrigenic helium, after subtracting possible tritogenic helium-3.

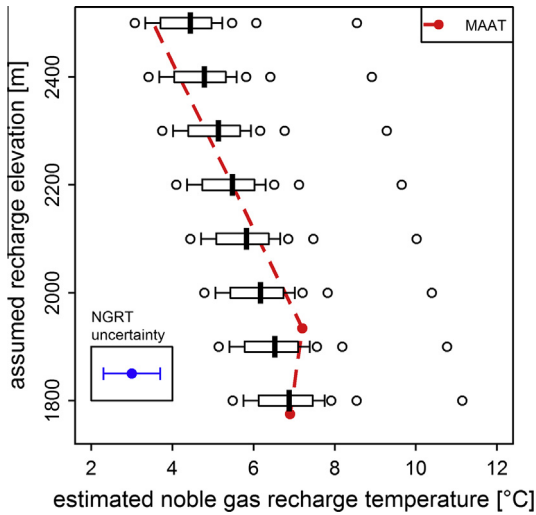


Fig. 3. Box-whisker plots, indicating the statistical distribution of the derived noble gas recharge temperatures (NGRT) of all samples, estimated using the Closed Equilibrium (CE) model.) The ranges show how the derived noble gas recharge temperature depends on the assumed recharge elevation. Open circles represent outliers. Red dots represent mean annual air temperature (MAAT) at the valley floor (1775 m, 6.9 °C) and Truckee #2 Snotel station (1943 m, 7.2 °C). Dashed line represents interpolated MAAT and adiabatic lapse rate for higher elevations. Blue inset indicates to scale the propagated uncertainty (0.7 °C) of the estimated NGRT. (For interpretation of the references to color in this figure legend, the reader is referred to the web version of this article.)

Flow depths are shown as arrows on the cross section in Fig. 5. Because both calculated recharge temperatures and calculated mean flow depths involve several assumptions, the arrows are not intended to be precisely determined mean flow depths, but rather an indication of the source depth of the sampled groundwater. Well K, one of the valley’s most productive wells, has a calculated flow depth near the estimated maximum depth to bedrock. This well also has a groundwater age of greater than 50 years, as demonstrated by the absence of tritium, consistent with the long

flow path and residence time inferred from the deep flow depth. The overall pattern is that the modeled mean flow depth generally increases towards the lower elevations of the valley floor. To test whether the estimated flow depth was a better predictor for the source of the groundwater than average screen depth, electrical conductivity and tritium concentration were plotted against both the average depth of the perforated sections and the calculated flow depth (Fig. 6). Electrical conductivity (Fig. 6a) was found to increase with increasing flow depths ($R^2 = 0.45$), likely because longer flow paths provide a longer time period for water–rock interaction. In contrast, electrical conductivity was found to decrease with depth when plotted against the average well depth while the correlation coefficient (R^2) was only 0.09.

Wells with shallower flow depths also contain higher tritium concentrations (Fig. 6b, $R^2 = 0.61$). The same trend is found when tritium is plotted against average screen depth, but with a much lower correlation coefficient ($R^2 = 0.09$).

The calculation of circulation depth from the discharge temperature is based on the assumption of uniform thermal conditions, which may or may not be an appropriate assumption. The subsurface temperature distribution may be heterogeneous when moving from areas of recharge (downward flow causing depressed subsurface temperatures) to areas of discharge (upward flow causing elevated subsurface temperatures). However, if strong vertical flow velocities alter the geothermal gradient, the estimated flow depth still represents the source depth of the sampled groundwater. Upward flow causing elevated subsurface temperatures will lead to higher discharge temperatures, larger differences with the recharge temperature and therefore a deeper estimated flow depth, reflecting the deeper source of the groundwater sample. Downward flow causing depressed subsurface temperatures will lead to lower discharge temperatures, smaller differences with the recharge temperatures and therefore a shallower estimated flow depth, reflecting the shallower source of sampled groundwater. The correlations between electrical conductivity and tritium and flow depth confirm that the flow depth derived from the temperature difference between recharge and discharge is a useful parameter for investigating the flow history of a groundwater

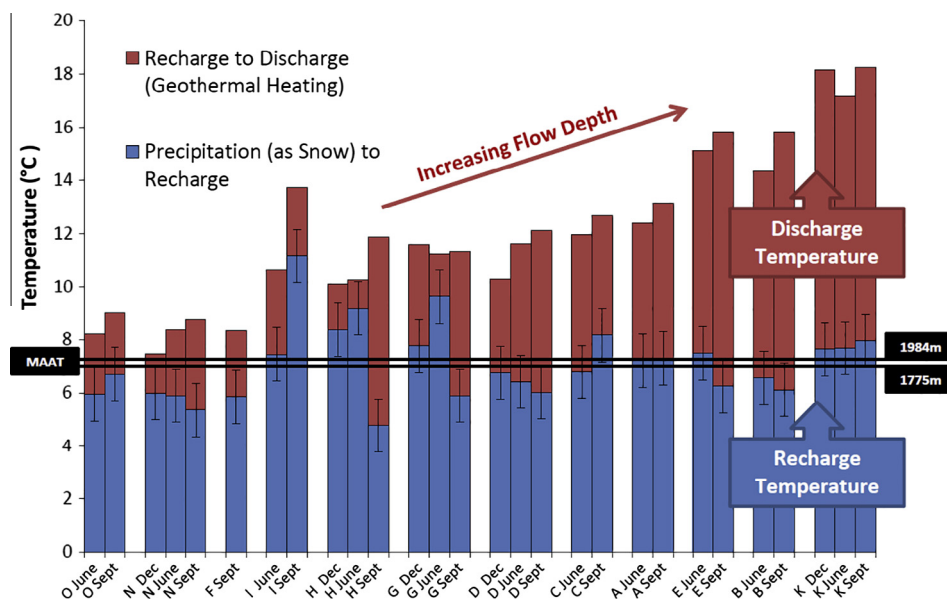


Fig. 4. Groundwater recharge and discharge temperatures in Martis Valley. Noble gas recharge temperatures, measured discharge temperatures, and mean annual air temperature are plotted for Martis Valley groundwater wells in order of increasing flow depth. Recharge temperatures in Martis Valley are higher than expected for direct infiltration of snowmelt. Most recharge temperatures fall near the mean annual air temperatures at elevations between 1775 m and 1984 m, indicating that most recharge occurs within a soil zone between these elevations.

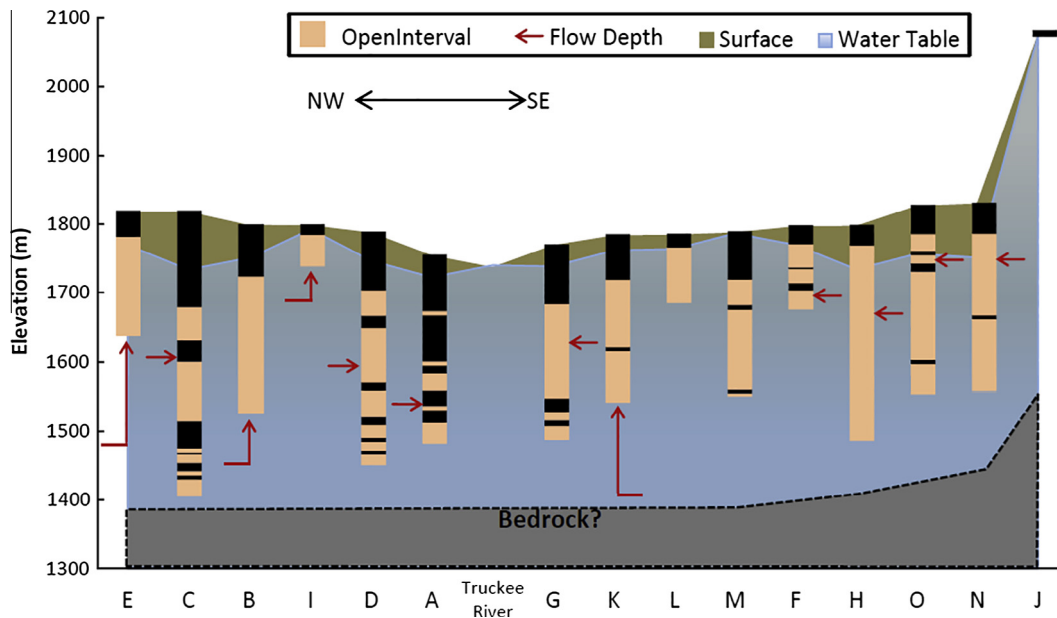


Fig. 5. Schematic cross section showing well screen intervals, calculated average flow depth assuming a geothermal gradient of 25 °C/km (see discussion in text), and the water table. The cross-section is an approximate projection of the wells shown in Fig. 1. Depth to bedrock is approximate and based on the maximum reported depth (Fram et al., 2009).

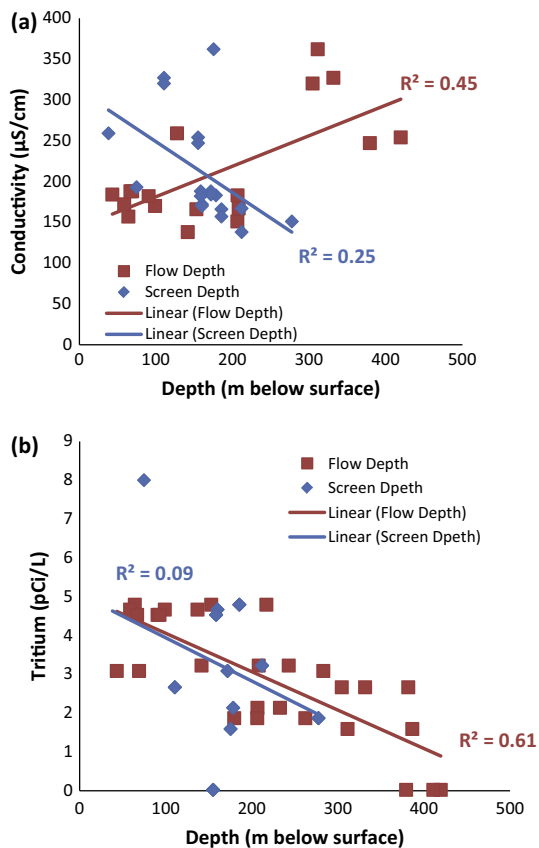


Fig. 6. Groundwater conductivity (a) and tritium concentration (b) against average screen depth (blue) and calculated mean flow depth (red) in Martis Valley wells. A positive correlation is observed between specific conductance and calculated mean flow depth. Wells with shallower flow paths contain younger groundwater and higher average tritium concentrations, suggesting younger water is likely the driver of seasonal groundwater variability. (For interpretation of the references to color in this figure legend, the reader is referred to the web version of this article.)

sample. Comparing NGRTs and discharge temperatures shows promise for examining mean, integrated flow-depths in thick aquifer sequences, but requires much more study in samples with better depth control, and supporting evidence from groundwater modeling or additional environmental tracers.

3.4. Mantle helium in Martis Valley groundwater

Martis Valley is a structural basin in the Walker Lane Belt shear zone, a transitional zone between the Sierra Nevada Mountains and the Basin and Range Geomorphic Provinces (Brown and Caldwell, 2013). Active tectonics is associated with additional crustal and mantle helium components. Many of the groundwater samples have concentrations of helium in excess of atmospheric solubility equilibrium and excess air. The source of excess helium can be examined by plotting helium isotopic composition against helium concentration, after correcting both for the excess air component (by subtracting excess air helium) and after normalizing the groundwater helium concentration to the equilibrium solubility helium concentration. In practice, one plots groundwater $^3\text{He}/^4\text{He}$ (corrected for excess air) against the ratio of equilibrium atmospheric ^4He concentration to groundwater ^4He concentration (corrected for excess air) (Saar et al., 2005). Such a plot for Martis Valley wells (Fig. 7) shows that the excess helium in Martis Valley groundwater is composed of a mixture of mantle and radiogenic helium. On this plot, atmospheric helium plots at 1, 1. Tritium decay increases the groundwater $^3\text{He}/^4\text{He}$ ratio but does not affect the ^4He concentration, and so moves the atmospheric value straight up, parallel to the y-axis. Addition of radiogenic helium from U/Th decay in the crust results in a lower $^3\text{He}/^4\text{He}$ composition because the helium isotope ratio of radiogenic helium is 1.5% of atmospheric (2×10^{-8}) (Torgersen, 1980).

The addition of mantle helium, having a $^3\text{He}/^4\text{He}$ ratio of 8 ± 2 (Craig et al., 1978) times atmospheric, results in an increased groundwater helium to isotopic composition. The presence of radiogenic and mantle helium in Martis Valley groundwater samples can be assessed by examining samples that have little or no tritogenic helium, i.e. samples with tritium concentrations of

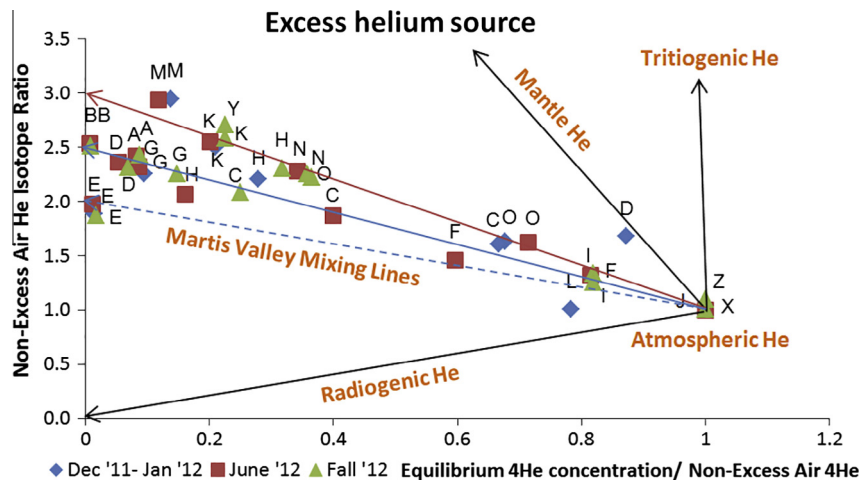


Fig. 7. By plotting the non-excess air $^3\text{He}/^4\text{He}$ ratio to atmospheric $^3\text{He}/^4\text{He}$ versus the equilibrium ^4He concentration/ non-excess air ^4He , the source of excess helium in Martis Valley is identified as a mixture of mantle and radiogenic helium. The proportions of these mixtures vary spatially. Wells in northern and northeastern Martis Valley contain less mantle helium and plot along the blue and dashed-blue mixing lines. The position along the mixing line gives a rough indication of groundwater age. Younger samples plot closer to the atmospheric He end member and older samples plot towards the Y intercept. (For interpretation of the references to color in this figure legend, the reader is referred to the web version of this article.)

<1 pCi/L and groundwater ages in excess of 50 years. In Fig. 7, wells K, M, and Y plot on a mixing line (shown in red in Fig. 7) with an intercept of 3.0. The sources of excess helium for these samples are 35–40% mantle helium, and 60–65% radiogenic helium. Most wells in southern Martis Valley plot along this red mixing line. Most wells in the northern Martis Valley plot along a lower (blue in Fig. 7) line, suggesting that less mantle helium is present in this area. There is a possible third mixing line (shown in dashed blue in Fig. 7), for wells in northeast Martis Valley with a lower fraction of mantle helium. Table 2 lists the isotope ratio of the non-atmospheric helium component (tritogenic and terrigenic) as well as the minimal isotope ratio of the terrigenic component after subtracting all possible tritogenic helium (assuming the observed tritium concentration recharged 55 years ago and has since accumulated tritogenic helium).

Determining the groundwater age of samples that plot along these lines is difficult because the calculation of tritogenic helium is highly sensitive to estimated isotopic composition of the terrigenic (mantle + radiogenic) helium component (Mahara et al., 2009).

3.5. Groundwater residence times

A key finding of the study is the presence of tritium above the detection limit in all but three wells and one spring. The presence of tritium above the detection limit in most groundwater samples from Martis Valley provides important evidence for the pervasive presence of a component of recent recharge.

In contrast to wells containing the young water indicators, wells K, L, M and Spring Y, have tritium concentrations of <1 pCi/L and are listed in Table 2 as having $^3\text{H}/^3\text{He}$ ages “>50 years”. These wells are located near the basin depocenter and likely produce water exclusively from the deeper, confined aquifer system. Although the deeper aquifer cannot be clearly delineated based on wellbore data, the fact that wells near the basin depocenter were originally artesian, in combination with noble gas, tritium results, and discharge temperature, all indicate deep sources and a long residence time for groundwater issuing from this portion of the basin.

An accurate determination of the tritogenic ^3He concentration is needed in order to calculate a meaningful tritium–helium groundwater age. In most groundwater, mantle helium is not present and the contribution to ^3He from radiogenic helium, which has

a low $^3\text{He}/^4\text{He}$ of 2×10^{-8} (Torgersen, 1980) relative to the atmospheric ratio of 1.384×10^{-6} , is small and can be accounted for. The presence of even small amounts of mantle helium, which has a $^3\text{He}/^4\text{He}$ ratio 6–10 times higher than the atmospheric ratio (Craig et al., 1978), makes it difficult to distinguish mantle ^3He from tritogenic ^3He . A further complication is that while production of radiogenic helium can be assumed to be relatively uniform for a given basin, the spatial distribution of mantle helium can be highly heterogeneous. Wells containing >1 pCi/L tritium and labeled as “mantle He” in Table 2 have a component of water with an average age of less than 50 years, but exact ages cannot be determined due to the presence of mantle helium. For samples with low concentrations of terrigenic helium, less than 50% of the atmospheric equilibrium concentration, the $^3\text{H}/^3\text{He}$ age was calculated after removing terrigenic helium with an assumed isotope ratio of 2.5 ± 0.5 times atmospheric. The terrigenic helium isotope ratio uncertainty was incorporated in the calculation of the $^3\text{H}/^3\text{He}$ age uncertainty.

Sources of mantle helium are generally deep-seated, so flow paths require conduits that bring deep water into shallower systems, a process that enhances mixing of water masses with differing residence times. The concentration of terrigenic (mantle + radiogenic) helium can be used to identify very old water components, i.e. samples with concentrations of terrigenic ^3He in excess of 50% of atmospheric concentrations are identified as containing a portion of groundwater that is greater than a thousand years old. The accumulation rate of radiogenic ^3He in groundwater depends on the production of radiogenic ^3He (related to the concentrations of uranium and thorium in the aquifer sediments), and the porosity. Typical U and Th concentrations support a production rate of $2 \mu\text{cm}^3$ (STP) per m^3 rock per year. Accumulation rates two orders of magnitude higher have been observed in fine grained sediments due to the release of accumulated ^4He in the sediment grains (Solomon et al., 1996). Here, we assumed an accumulation rate of $2 \times 10^{-11} \text{cm}^3$ (STP)/(g year), based on a porosity of 0.1. In order to classify samples according to their residence times, we use the fact that groundwater samples with tritium concentrations of greater than 1 pCi/L contain a portion of groundwater that has a subsurface residence time of less than 50 years. Then, plotting terrigenic ^4He versus tritium concentrations (Fig. 8) shows whether the groundwater is young, intermediate, old or mixed age. Groundwater age classifications are shown in Table 3.

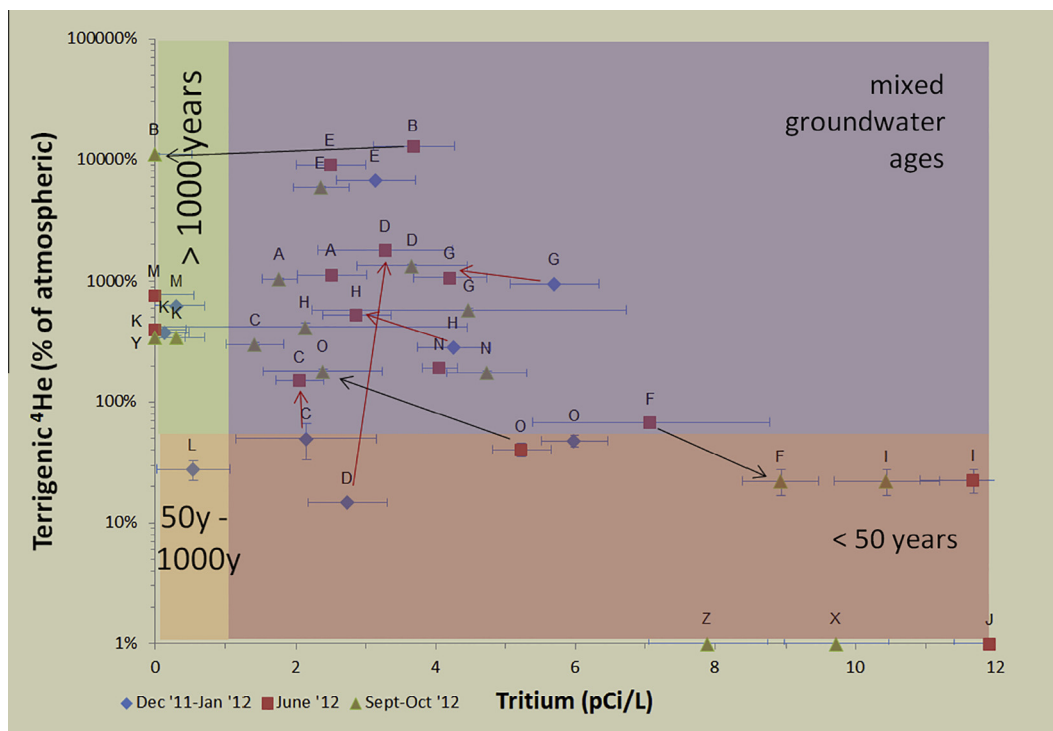


Fig. 8. Groundwater age mixing in Martis Valley groundwater: tritium and terrigenous helium. The four groundwater age classifications outlined in Table 3 are shown as shaded regions on this plot; symbols indicate sampling season and individual wells are labeled with their letter A–O designations. Red arrows show significant changes in groundwater composition from winter to summer; black arrows show changes from summer to fall. The data show that the groundwater produced by Martis Valley production wells varies seasonally in the proportion of younger water (with high tritium and low terrigenous ^4He) and older water (with low tritium and high terrigenous ^4He) produced. (For interpretation of the references to color in this figure legend, the reader is referred to the web version of this article.)

Table 3
Groundwater age classification.

Classification	Age range (year)	Tritium	Terrigenous He	# of samples
Young	<50	Yes (>1 pCi/L)	Low (<50% excess He)	10
Intermediate-age	50–1000	No (<1 pCi/L)	Low (<50% excess He)	1
Old	>1000	No (<1 pCi/L)	High (>50% excess He)	7
Mixed-age	Mixed	Yes (>1 pCi/L)	High (>50% excess He)	20

3.6. Seasonal variation in groundwater residence time indicators and climate change vulnerability

Most of the wells in Martis Valley produce groundwater with a mixed age as expected in wells with long and multiple well screen intervals (Fig. 8). The degree of mixing between the three age groups is indicated by a sample's position in the mixed-age section of the graph. Many of the wells sampled during multiple sampling events showed a seasonal variation in the proportions of different groundwater sources that compose their mixed groundwater age.

The changing proportions of different groundwater sources lead to changes in tritium and terrigenous helium concentrations, representing the modern and old groundwater components. To investigate these seasonal changes, the concentrations differences from the summer 2012 concentration are plotted in Fig. 9. Positive bars show that the winter or fall concentrations were higher than the summer concentration, negative bars show that the summer concentration was higher. Four wells (G, H, N and O) had significantly (1σ) higher tritium concentrations in winter 2011 than in summer 2012. Three wells (B, C, I) showed lower tritium concentrations in fall than in summer (Fig. 9a). The wells with the highest groundwater source seasonal variability generally have shallower average flow depths. In contrast to the tritium concentrations, terrigenous

helium concentrations in all wells were significantly different (2σ) between the winter and summer sampling and also between the summer and fall sampling, except for well I. Samples collected in summer contained higher concentrations than both winter and fall samples for all wells except C and O. Combined with the lower concentrations of tritium in summer compared to winter, this indicates that wells abstract a larger proportion of older groundwater during summer and that the youngest water is depleted from the well capture zone through pumping and natural discharge by fall. A similar phenomenon was observed in nearby Olympic Valley, where groundwater ages increased from 0–2 years in spring/early summer to 4–6 years in September (Singleton and Moran, 2010).

This is additional evidence that differing amounts of younger water is likely the driver of seasonal groundwater variability. Wells sampling younger water (shallower flow paths) are more likely to change seasonally because they sample different flow depths at different times of the year. Because different groundwater sources will have different flow paths to a given receptor, tritium concentrations are expected to change due to differences in both initial tritium at the time of recharge and in the amount of radioactive decay during transport along shorter or longer flow paths. Differences in tritium concentration likely reflect differences in proportions of younger and older groundwater in mixtures from the wells. In this case, dif-

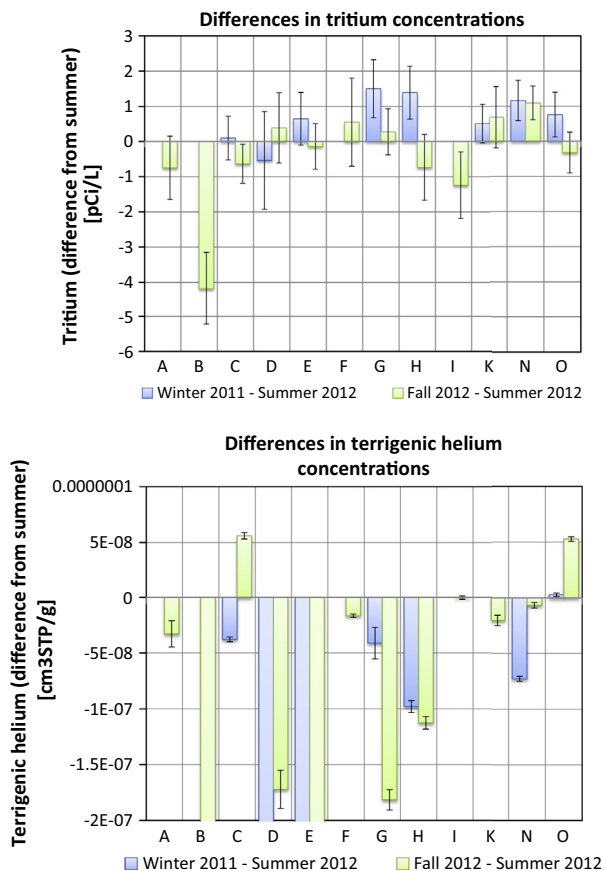


Fig. 9. Seasonal variability in tritium (a) and terrigenous helium (b) concentrations. Variations are calculated as the difference from values determined for “Summer” samples collected in June 2012. Error bars represent the combined uncertainty for the difference in values. “Winter” samples were collected December 2011–January 2012. “Fall” samples were collected from September 2012–October 2012.

ferences in terrigenous helium concentrations appeared much more sensitive to the mixing of younger and older groundwater.

Martis Valley groundwater recharge temperatures indicate that groundwater recharge in Martis Valley is occurring primarily in the lower part of the watershed. Climate change is likely to significantly impact this pattern over the next several decades. With the snowmelt hydrograph shifted to an earlier and sharper peak (Earman and Dettinger, 2007), groundwater recharge of snowmelt will likely decrease, and runoff to the Truckee River will likely increase, increasing the potential for flooding. A greater proportion of precipitation falling as rain may mitigate some of the negative impacts on recharge and mitigate or exacerbate the negative impacts on flooding, depending on the intensity of the rainfall events. For example, rain falling on exposed soil or rock at an intensity less than the historical rate of snowpack melting would be more likely to contribute to recharge. However, the effects of evapotranspiration under a warmer climate are complex. A longer growing season would inhibit percolation and recharge but higher soil water content when potential evapotranspiration is lower would enhance infiltration.

The seasonal variations in tritium and especially in terrigenous helium found in mixed groundwater show that some wells are producing a significant component of younger groundwater during certain times of the year. Wells with the shallowest calculated flow depths and multiple lines of evidence for a component of recent recharge also show the greatest seasonal variability in groundwater source, and are likely to be the first to be affected by climate-driven change in recharge patterns.

4. Summary and conclusions

Dissolved noble gases and isotopes are useful in evaluating the vulnerability of alpine basin groundwater to climate change because they can be applied to answering key questions about recharge location and groundwater residence time. In Martis Valley, most of the groundwater recharge is probably occurring at the valley floor in alluvial deposits or from infiltration via streams.

Martis Valley is predicted to experience major changes in hydrologic conditions due to climate change. In this study, we found that long screened wells produce groundwater with mixtures of ages, from less than 50 years (containing tritium) to over 1000 years (containing terrigenous helium). Establishing a better defined age distribution requires a combination of age tracers (Visser et al., 2013a). Seasonal variations in recharge temperatures, tritium, and excess air suggest that the wells capture water masses of varying recharge conditions and groundwater ages throughout the year. Wells with shallow flow depths show significant seasonal variability, making them particularly vulnerable to changes in the amount, timing, and location of recharge.

Higher temperatures will bring an increase in the elevation of the snowline and potentially more rain at the elevations where most recharge occurs. Instead of most recharge occurring during the time of snowmelt runoff, recharge of rain may be spread over a longer time period during the winter months. High intensity precipitation will lead to high runoff and low infiltration, but low intensity precipitation could lead to higher infiltration rates, if the rainfall rate is less than the current rate of snowpack melting. In either case, recharge of snowmelt runoff is likely to decrease, since it is predicted to be of lower volume and take place over a shorter time period.

In comparing results from this study to those from nearby Olympic Valley (Singleton and Moran, 2010), some similarities are the approximate elevation of most recharge, little evidence of mountain block recharge, and the presence of recent recharge in production wells. However, the residence time of water in Olympic Valley wells is in general much shorter, likely due to the much smaller storage volume of the Olympic Valley basin sediments (estimated at $1.8 \times 10^7 \text{ m}^3$) compared to Martis Valley basin sediments (estimated at $6.0 \times 10^8 \text{ m}^3$). In both basins, water is produced from multiple flow paths having a mixture of ages and sources. The proportions of these different groundwater sources vary seasonally and will likely differ in the timescale of climate change impacts and overall sustainability.

Acknowledgements

The authors are grateful to the well owners and water agencies who cooperated with the research, including Truckee Donner Public Utility District, Placer County Water Agency, and Northstar Community Services District. Fruitful discussions were held with Justin Huntington and Matt Reeves of the Desert Research Institute on the hydrology and hydrogeology of the Martis Valley Basin. We gratefully acknowledge three anonymous reviewers for their constructive comments that helped us improve the quality of our paper. Part of this work was performed under the auspices of the U.S. Department of Energy by Lawrence Livermore National Laboratory under Contract DE-AC52-07NA27344. LLNL-JRNL-645078.

References

- Aeschbach-Hertig, W., Peeters, F., Beyerle, U., Kipfer, R., 2000. Palaeotemperature reconstruction from noble gases in ground water taking into account equilibration with entrapped air. *Nature* 405 (6790), 1040.
- Aeschbach-Hertig, W., El-Gamal, H., Wieser, M., Palcsu, L., 2008. Modeling excess air and degassing in groundwater by equilibrium partitioning with a gas phase. *Water Resour. Res.* 44 (8).

- Aguilera, H., Murillo, J., 2009. The effect of possible climate change on natural groundwater recharge based on a simple model: a study of four karstic aquifers in SE Spain. *Environ. Geol.* 57 (5), 963–974.
- Ajami, H., Meixner, T., Dominguez, F., Hogan, J., Maddock 3rd, T., 2012. Seasonalizing mountain system recharge in semi-arid basins-climate change impacts. *Ground Water* 50 (4), 585–597.
- Barthel, R. et al., 2009. Integrated assessment of groundwater resources in the Oueme basin, Benin, West Africa. *Phys. Chem. Earth* 34 (4–5), 236–250.
- Brown & Caldwell, 2013. Martis Valley Groundwater Management Plan. California Department of Water Resources, 2006. Martis Valley Groundwater Basin.
- Clarke, W.B., Jenkins, W.J., Top, Z., 1976. Determination of tritium by mass spectrometric measurement of ^3He . *Int. J. Appl. Radiat. Isot.* 27 (9), 515–522.
- Coats, R., 2010. Climate change in the Tahoe basin: regional trends, impacts and drive. *Clim. Change* 102 (3–4), 435–466. <http://dx.doi.org/10.1007/s10584-010-9828-3>.
- Coulter, T., et al., 2009. Truckee River Operating Agreement Final EIS/EIR.
- Craig, H., Lupton, J.E., Welhan, J.A., Poreda, R., 1978. Helium isotope ratios in Yellowstone and Lassen Park volcanic gases. *Geophys. Res. Lett.* 5 (11), 897–900.
- Dean Ruyan Associates, 2013. California travel impacts by county, 1992–2011 2012 preliminary state and regional estimates. In: C.T.a.T. (Ed.), Commission.
- Earman, S., Dettinger, M., 2007. Long-Term Recharge Change in the Mountains of California and Nevada.
- Ekwurzel, B., 2004. LLNL Isotope Laboratories Data Manual, Version 12, Lawrence Livermore National Laboratory, UCRL-TM-203316.
- Flint, A.L., Flint, L.E., Dettinger, M.D., 2008. Modeling soil moisture processes and recharge under a melting snowpack. *Vadose Zone J.* 7 (1), 350.
- Fram, M., Munday, C., Belitz, K., 2009. Groundwater Quality Data for the Tahoe – Martis Study Unit, 2007: Results from the California GAMA Program.
- Green, T.R. et al., 2011. Beneath the surface of global change: impacts of climate change on groundwater. *J. Hydrol.* 405 (3–4), 532–560.
- Heaton, T.H.E., Vogel, J.C., 1981. “Excess air” in groundwater. *J. Hydrol.* 50, 201–216.
- Hunter, L.E., Howle, J.F., Rose, R.S., Bawden, G.W., 2011. LiDAR-assisted identification of an active fault near Truckee, California. *Bull. Seismol. Soc. Am.* 101 (3), 1162–1181.
- Huntington, J.L., et al., 2013. Integrated Hydrologic Modeling of Lake Tahoe and Martis Valley Mountain Block and Alluvial Systems, Nevada and California.
- Hydro-Search, I., 1995. Ground Water Management Plan Phase 1 Martis Valley Ground-Water Basin No. 6–67 Nevada and Placer counties, California. Prepared for Truckee Donner Public Utility District January 31, 1995.
- Ingram, R.G.S., Hiscock, K.M., Dennis, P.F., 2007. Noble gas excess air applied to distinguish groundwater recharge conditions. *Environ. Sci. Technol.* 41 (6), 1949–1955.
- Kleppe, J.A. et al., 2011. Duration and severity of Medieval drought in the Lake Tahoe Basin. *Quaternary Sci. Rev.*
- Mahara, Y. et al., 2009. Groundwater dating by estimation of groundwater flow velocity and dissolved ^4He accumulation rate calibrated by ^{36}Cl in the Great Artesian Basin, Australia. *Earth Planet. Sci. Lett.* 287 (1–2), 43–56.
- Manga, M., Kirchner, J.W., 2004. Interpreting the temperature of water at cold springs and the importance of gravitational potential energy. *Water Resour. Res.* 40 (W05110).
- Manning, A.H. et al., 2012. Evolution of groundwater age in a mountain watershed over a period of thirteen years. *J. Hydrol.* 460–461, 13–28.
- National Climatic Data Center, 2011. Annual Summaries Station Details: TRUCKEE RANGER STATION, CA US.
- National Resources Conservation Service, 2013. Truckee #2 Snotel station.
- Nimbus Engineers, 2001. Ground Water Availability in the Martis Valley Ground Water Basin.
- Novicky, O., Kasperek, L., Uhlik, J., 2010. Vulnerability of groundwater resources in different hydrogeology conditions to climate change. Taylor and Francis Group, CRC Press, London, UK.
- Poreda, R.J., Cerling, T.E., Solomon, D.K., 1988. Tritium and helium-isotopes as hydrologic tracers in a shallow unconfined aquifer. *J. Hydrol.* 103 (1–2), 1–9.
- Saar, M.O., Castro, M.C., Hall, C.M., Manga, M., Rose, T.P., 2005. Quantifying magmatic, crustal, and atmospheric helium contributions to volcanic aquifers using all stable noble gases: implications for magmatism and groundwater flow. *Geochem. Geophys. Geosyst.* 6 (3).
- Schlosser, P., Stute, M., Dorr, H., Sonntag, C., Munnich, K.O., 1988. Tritium/ ^3He dating of shallow groundwater. *Earth Planet. Sci. Lett.* 89 (3–4), 353–362.
- Singleton, M.J., Moran, J.E., 2010. Dissolved noble gas and isotopic tracers reveal vulnerability of groundwater in a small, high-elevation catchment to predicted climate changes. *Water Resour. Res.* 46 (12).
- Solomon, D.K., Hunt, A., Poreda, R.J., 1996. Sources of radiogenic helium-4 in shallow aquifers: Implications for dating young groundwater. *Water Resour. Res.* 32, 1805–1813.
- Stone, M., Lopez, H., 2009. Potential Climate Change and Impacts on Water Resources.
- Stute, M., Clark, J.F., Schlosser, P., Broecker, W.S., Bonani, G., 1995a. A 30,000 year continental paleotemperature record derived from noble gases dissolved in groundwater from the San Juan Basin, New Mexico. *Quaternary Res.* 43 (2), 209.
- Stute, M. et al., 1995b. Cooling of tropical Brazil (5 °C) during the last glacial maximum. *Science (New York, N.Y.)* 269, 379–383.
- Surano, K.A. et al., 1992. Helium-3 mass spectrometry for low-level tritium analysis of environmental samples. *J. Radioanal. Nucl. Chem.* 161 (2), 443–453.
- Takaoka, N., Mizutani, Y., 1987. Tritogenic ^3He in groundwater in Takaoka. *Earth Planet. Sci. Lett.* 85 (1–3), 74–78.
- Torgersen, T., 1980. Controls on pore-fluid concentration of He-4 and Rn-222 and the calculation of He-4–Rn-222 ages. *J. Geochem. Explor.* 13, 57.
- Visser, A., Broers, H.P., Purtschert, R., Sültenfuß, J., de Jonge, M., 2013a. Groundwater age distributions at a public drinking water supply well field derived from multiple age tracers (^{85}Kr , $^3\text{H}/^3\text{He}$, and ^{39}Ar). *Water Resour. Res.* 49 (11), 7778–7796.
- Visser, A. et al., 2013b. A membrane inlet mass spectrometry system for noble gases at natural abundances in gas and water samples. *Rapid Commun. Mass Spectr.* 27 (21), 2472–2482.
- Wilson, G.B., McNeill, G.W., 1997. Noble gas recharge temperatures and the excess air component. *Appl. Geochem.* 12 (6), 747–762.